Materials Today Physics 35 (2023) 101098

Contents lists available at ScienceDirect

Materials Today Physics

journal homepage: www.journals.elsevier.com/materials-today-physics

Air-sensitive amplified spontaneous emission in lecithin-capped $CsPbBr_3$ nanocrystals thin films

Stefania Milanese [a,1], Giovanni Morello [b,c,1], Maria Luisa De Giorgi [a,*], Arianna Cretì [b], Hordii Andrusiv [d,e], Maryna I. Bodnarchuk [d,e], Antonio Qualtieri [c], Mauro Lomascolo [b], Maksym V. Kovalenko [d,e], Marco Anni [a]

[a] Dipartimento di Matematica e Fisica "Ennio De Giorgi", Università Del Salento, Via per Arnesano, 73100, Lecce, Italy
[b] CNR IMM – Institute for Microelectronics and Microsystems - Unit of Lecce, Via per Monteroni, 73100, Lecce, Italy
[c] Center for Biomolecular Nanotechnologies @UNILE, Istituto Italiano di Tecnologia, Via Barsanti, I – 73010, Arnesano (LE), Italy
[d] Institute of Inorganic Chemistry, Department of Chemistry and Applied Biosciences, ETH Zürich, CH-8093, Zürich, Switzerland
[e] Laboratory for Thin Films and Photovoltaics, Empa – Swiss Federal Laboratories for Materials Science and Technology, CH-8600, Dübendorf, Switzerland

ARTICLE INFO

Keywords:
Amplified spontaneous emission
Perovskite
Sensing
Nanocrystals thin films

ABSTRACT

Fully inorganic lead halide perovskite nanocrystals (NCs) are receiving great attention as active materials for photonic and optoelectronic devices. While the lack of long-term stability, due to their sensitivity to ambient air exposure, currently prevents their application to commercial devices, the presence of reversible environmental effects opens the way for possible applications of lead halide perovskites in resistive or optical sensors. In this work we investigate the Amplified Spontaneous Emission (ASE) properties and their dependence on the surrounding environment of lecithin-capped $CsPbBr_3$ NCs thin films. We demonstrate low ASE threshold under nanosecond pumping, both in air and in vacuum, with emission intensity lower in air than in vacuum. We also show that the emission quenching induced by ambient air exposure, ascribed to moisture-induced surface solvation, is reversible and it is fully restored by a suited vacuum stint application. The ASE sensitivity is up to 6.5 larger than the spontaneous emission one, making lecithin-capped $CsPbBr_3$ NCs thin films promising systems for the development of optical humidity sensors with high sensitivity.

1. Introduction

Over the past few years lead halide perovskites have caught the attention of several researchers due to their advanced optical properties allowing their application as active materials in several optoelectronic devices, spanning from high efficiency solar cells [1] to LEDs [2], photodetectors [3] and lasers [4,5]. However, the application of perovskites in commercial devices is currently limited by their strong tendency to rapidly degrade; due to their high sensitivity to external environment, perovskites react to the presence of gases, light, moisture and heat, often resulting in an irreversible degradation of the material [6]. To overcome this drawback, several strategies have been tested like acting on the chemical structure [7,8], changing the deposition techniques [9–11], controlling the surface morphology and the dimensionality of the active material [12,13] or through post-deposition processes [14,15].

Recently some studies evidenced that reversible interactions with the environment are possible, that can be exploited for sensing applications. For example, thermal annealing has been demonstrated to reverse the phase transformation and the degradation process induced by water vapor [16–18]; in other cases, self-healing processes have been observed after photo-bleaching [19–22]. Moreover, the interaction with the environment has been demonstrated to induce reversible modulation of both the electrical conductance [23,24] and the emitted photoluminescence [25–27], opening the route for the development of resistive and optical sensors.

Among the different lead halide perovskite active systems, fully inorganic perovskites are particularly interesting due to their improved stability with respect to their hybrid counterpart. In presence of water hybrid methylammonium-based perovskites tend to hydrolyse, transforming the $CH_3NH_3^+$ ion in the corresponding CH_3NH_2 amine, leading to the complete degradation of the active material [28,29]. Replacing the common organic site with an inorganic one (such as caesium) makes

* Corresponding author.
E-mail address: marialuisa.degiorgi@unisalento.it (M.L. De Giorgi).
[1] First authors: Stefania Milanese and Giovanni Morello.

https://doi.org/10.1016/j.mtphys.2023.101098
Received 3 February 2023; Received in revised form 24 March 2023; Accepted 25 April 2023
Available online 25 April 2023

the perovskite less hydrophilic and more thermally stable [30,31], thus decreasing the decomposition rate and prolonging the lifetime of a potential device.

In addition, perovskite colloidal NCs are particularly interesting due to the easy bandgap energy tuning over the entire visible range via chemical composition and size control [9], ligand engineering for enhanced thermal and environmental stability [32], and low-cost and rapid film deposition techniques such as drop-casting or spin coating [33].

In order to ensure a good surface passivation and a long-term stability to the perovskite nanostructures, the choice of the ligand engineering approach is currently one of the most important challenges. To this aim, it has been demonstrated that long chain zwitterionic capping ligands, such as lecithin, help to control the nucleation and growth of perovskite crystals enhancing PL and electroluminescence stability [34]; moreover, lecithin molecules strong adhesion to the NC surface ensures stable and ultraconcentrated colloidal solutions [35] and prevents nanocrystals aggregation [36].

In the frame of developing active materials for efficient sensors, NCs thin films are particularly interesting thanks to their high surface-to-volume ratio, that allows a more efficient interaction with the gas analyte [37]. In particular, $CsPbBr_3$ NCs have attracted attention for optical devices thanks to their bright emission, high quantum yield and low threshold optical gain [38]. Moreover, $CsPbBr_3$ NCs have been seen to be sensitive to oxygen [39], ammonia [40], explosive vapors [37] and other volatile organic compounds [24], reacting to the presence of the external gas with a PL increase [41], quenching [37] or a conductance variation [24].

The role of the ambient gases on inorganic perovskite active films that lead to the modulation of the ASE intensity is instead almost unexplored to date, while being observed and demonstrated for other active materials. One of the first results comes from the experiments with semiconductor organic polymers for the detection of 2,4,6-trinitrotoluene (TNT) and 2,4-dinitrotoluene (DNT) explosive vapors [42], showing an ASE sensitivity up to 30 times higher than the Spontaneous Emission (SE) one. Furthermore, exploiting the ASE quenching as a sensitive method for formic acid vapors detection with MEH-PPV allowed to lower the limit of detection down to the sub-ppm range [43]. Finally, recently optical gain sensing has been exploited for humidity detection with CdSe/CdS core-shell QDs, allowing to obtain about 31 times enhancement in sensitivity [44].

In this work we study the ASE properties of lecithin-capped $CsPbBr_3$ nanocrystals films [35] and their dependence on the surrounding environment, namely ambient wet air and vacuum. First, we demonstrate optical gain with low ASE threshold, comparable with the state of art for nanosecond excitation regime [38], both in vacuum and ambient air conditions. Moreover, we show a clear sensitivity of the active material to the environment, noticeable as a reversible photoluminescence quenching in presence of air, with an enhanced sensitivity of ASE with respect to the spontaneous emission, up to 6.5 times. Finally, a full recovery of the photoluminescence intensity after few hours of dark storage, demonstrating an excellent self-healing character of caesium lead bromide nanocrystal films, is shown. Our results thus prove that fully inorganic NCs thin films are promising systems for the realization of efficient optical humidity sensors, based on ASE intensity modulation ascribed to moisture induced surface solvation.

2. Experimental section

2.1. Nanocrystals synthesis, film deposition and characterization

The synthesis of $CsPbBr_3$ NCs was conducted according to Ref [35] with some modifications as described below. In the synthesis of $CsPbBr_3$ NCs trioctylphosphine-Br_2 precursor was injected into the mixture of lead oleate and lecithin in octadecene at 130 °C under a nitrogen atmosphere. The reaction was cooled immediately by an ice bath. The crude solution was transferred into the glovebox and all purification steps were conducted in an inert atmosphere. First, the crude solution was centrifuged at 29500 g for 5 min. The precipitate was discarded and 16.5 mL of anhydrous ethyl acetate and acetone (2:1) were added to the supernatant followed by centrifugation at 29500 g for 5 min. The precipitate was dispersed in 0.6 mL of anhydrous toluene and used for further study. The concentration of the colloid was approx. 50–60 mg/mL.

Further details on the characterization of the nanocrystals (XRD, TGA, NMR spectroscopy) can be found in Ref. [35].

The optical absorption spectrum was measured with a Jasco V770 spectrometer in transmission mode. The photoluminescence spectrum was measured in a 90° configuration using a Horiba Fluoromax-4P + equipped with a photomultiplier tube and a monochromatized 150-W Xenon lamp as an excitation source. The NCs solution shows an absorbance spectrum with an excitonic peak at 505 nm and a PL spectrum with a peak at 512 nm (see Figure S1a).

TEM image was collected using a JEOL JEM2200FS microscope operating at 200 kV accelerating voltage. TEM image of the $CsPbBr_3$ NCs evidences cubic shaped NCs of about 10 nm in size (see Figure S1b).

The films have been deposited by drop casting 15 μL of NC solution (NC density ~ 3 mg/mL) on quartz substrates at room temperature under chemical hood. It shows a uniform morphology and a thickness of about 200 nm (see Figure S2).

The investigation of the prepared sample, in a cross-sectional view, has been performed by means of the dual-beam FEI Helios NanoLab 600i in order to assay its sub-micrometer thickness. In details, to inspect the cross-section, a 300 nm layer of Platinum has been deposited with a methylcyclopentadienyltrimethyl platinum source under 30 kV for Ga^+ ion acceleration and a beam current 40 pA. Then, a trench of about 3 μm as depth has been milled through the platinum with an ion current of 0.23 nA at a 52° tilting angle. The cross-section obtained has been imaged by electron-beam with 5 kV as acceleration voltage and a current of 0.34 nA.

The fluorescence maps have been recorded with an inverted fluorescence microscope (Nikon Eclipse C1), exciting the sample with a Hg-lamp in the 470–490 nm range, and collecting the fluorescence in the 520–560 nm range.

2.2. ASE measurements

ASE measurements have been performed by exciting the samples with a LBT MNL 100 Nitrogen laser, delivering 3 ns pulses at a wavelength of 337 nm, with a repetition rate of 10 Hz. The pump beam was focused onto the sample surface in a rectangular stripe (4 mm length, 80 μm width) in edge-pump configuration. The emission has been collected from the edge of the sample, dispersed by a 0.75 m focal length spectrograph (Acton 750), and analyzed by an Andor air-cooled Si CCD. The spectral resolution was 0.5 nm.

The experiments were carried out at room temperature by placing the sample in a vacuum chamber. Different pressure levels were used, between 10^{-1} mbar (hereafter referred as *vacuum* condition) and the atmospheric one, corresponding to wet air with about 60% of relative humidity (RH) (hereafter referred as *air* condition). The sample ASE properties have been investigated, in the two extreme conditions, by measuring the emission spectra as a function of the excitation density.

2.3. Spontaneous emission (SE) and amplified spontaneous emission (ASE) relative quenching

The role played by the atmosphere surrounding the NCs films on their emission properties has been investigated by defining the air induced relative quenching (RQ) as $\frac{\Delta I}{I} = \frac{I_{vac} - I_{air}}{I_{vac}} \times 100$ where I_{vac} represents the integrated intensity in vacuum and I_{air} the integrated intensity in air conditions. The ΔI/I ratio has been calculated both for the

spontaneous $\left(\frac{\Delta I}{I}\right)_{SE} = \frac{I_{vac_{SE}} - I_{air_{SE}}}{I_{vac_{SE}}} \times 100$ (RQ_{SE}) and the amplified spontaneous $\left(\frac{\Delta I}{I}\right)_{ASE} = \frac{I_{vac_{ASE}} - I_{air_{ASE}}}{I_{vac_{ASE}}} \times 100$ (RQ_{ASE}) emission.

The SE and ASE contributions to the total emission have been separated by subtracting from each spectrum above the ASE threshold a properly scaled spectrum measured below the threshold.

The sensitivity (S) of the device has been determined as the slope of the photoluminescence relative quenching dependence on the test chamber pressure, both for the spontaneous (S_{SE}) and amplified spontaneous (S_{ASE}) emission.

Limit Of Detection (LOD), which is the minimum humidity concentration that can be detected, was determined with a confidence level of 95% as the humidity concentration determining an intensity variation that differs from the blank value for two standard deviations. In our case the blank value corresponds to the intensity at the humidity concentration level of the higher vacuum condition (C = 4.2 ng/cm^3).

2.4. Time-resolved PL measurements

TR-PL measurements were performed exciting the samples by a solid-state pulsed laser (mod. PLP10-040, Hamamatsu), which provided pulses at a wavelength of 402 nm (3.08 eV) of about 58 ps, at a repetition rate of 1 MHz, with a maximum peak power of 70 mW. The PL was dispersed by an iHR320 (focal length of 0.32 m) Horiba monochromator equipped with a Peltier cooled Hamamatsu photomultiplier (Head-on mod R943-02), operating in single photon counting mode. The Time-Correlated Single Photon Counting (TCSPC) technique has been used to record TR-PL by using an Edinburg Instruments TCC900 TSCPC electronic card. The temporal resolution of the system was of about 0.46 ns. The experiments were carried out in vacuum (10^{-3} mbar) and wet air atmosphere, by putting the samples in a chamber connected to a vacuum-pump.

3. Results and discussion

First, we investigated the excitation density dependence of the emitted photoluminescence in vacuum condition, summarized in Fig. 1.

At low excitation density (see Fig. 1a) the PL spectrum shows a single spontaneous emission band peaked at about 525 nm, with a Full Width at Half Maximum (FWHM) of about 23 nm. As the excitation density increases, a progressive intensity growth is detected, accompanied with the appearance of a narrow band centered at about 531 nm at about 0.60 mJ cm^{-2}, progressively dominating the emission as the excitation density is further increased and ascribed to ASE. The ASE band appearance results in a superlinear increase of the output intensity with the excitation density (see Fig. 1c) and in the typical FWHM narrowing, as reported in Figure S3a. In this work, the ASE threshold is defined as the lowest excitation density that allows to observe the ASE induced line-shape variation, also defined as visual threshold [45].

The obtained threshold value is among the lowest to date reported in $CsPbBr_3$ NCs neat films under nanosecond pumping [46–48], evidencing excellent ASE properties of these lecithin-capped NCs. We also observe that the corresponding excitation power density (about 200 kW cm^{-2}) can be easily obtained with cheap pumping sources, like pulsed inorganic UV diodes [49].

The role of the environment on the optical properties of the sample

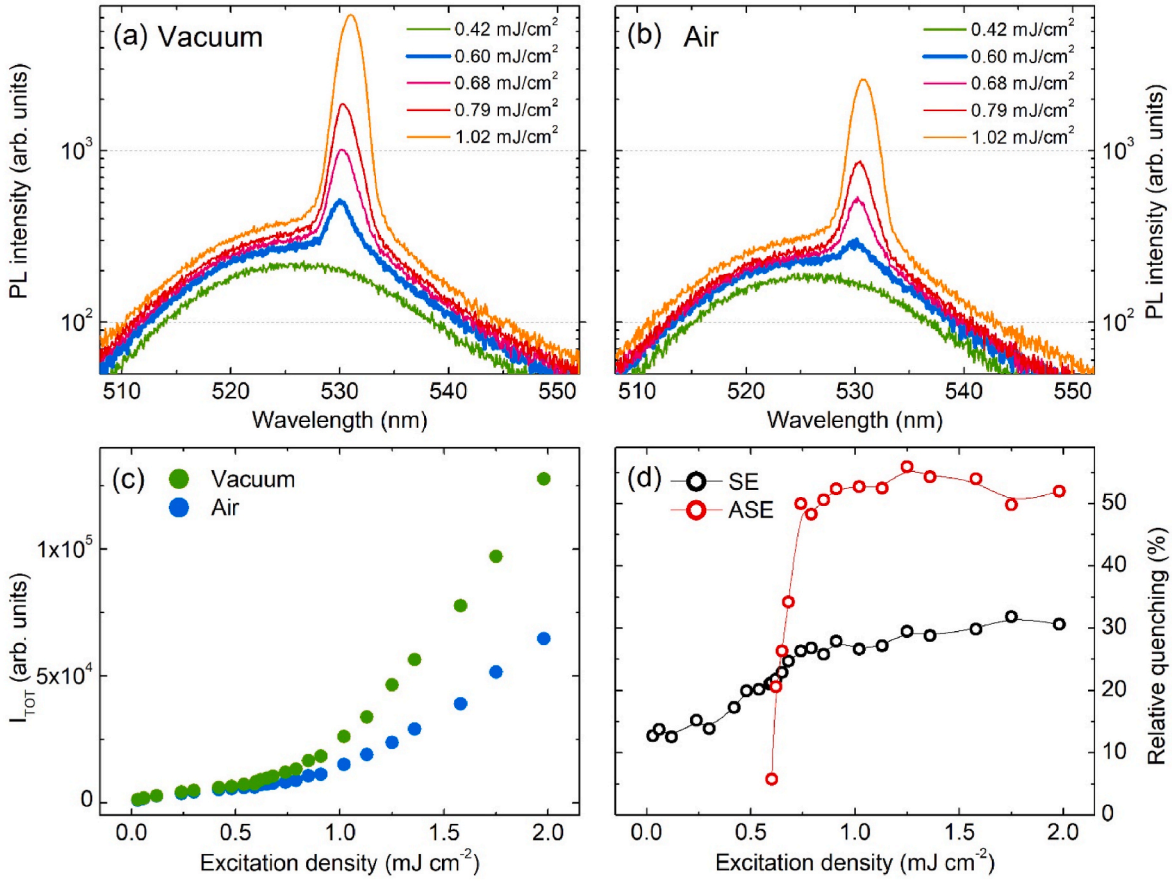

Fig. 1. Excitation density dependence of a selection of PL spectra in (a) vacuum and (b) air; the blue thicker lines evidence the PL spectra corresponding to the visual threshold. (c) Excitation density dependence of the PL intensity integrated over the entire sample emission spectral range in vacuum (green dots) and air (blue dots). (d) Spontaneous Emission (black circles) and Amplified Spontaneous Emission (red circles) integrated intensity RQ. (For interpretation of the references to color in this figure legend, the reader is referred to the Web version of this article.)

has then been investigated by performing the same kind of measurements when the NCs film was exposed to ambient air (60% RH). At low excitation density the spontaneous emission shows the same spectral line-shape and peak wavelength with respect to the vacuum one (see Fig. 1b). As the excitation density increases the appearance of the ASE band is still observed (see Fig. 1c and S2b), with a visual threshold similar to the one observed in vacuum, even if the lower intensity at 0.60 mJ cm^{-2} suggests a slightly higher threshold with respect to vacuum conditions (see Figure S4 in the Supporting Information for further details).

Beyond the slight threshold increase in air, our data clearly show that the total emission intensity in air is, at all the excitation densities, systematically lower than the one in vacuum (see Fig. 1c), clearly indicating the presence of an air-induced exciton quenching process. In order to quantify this effect, we determined the air-induced intensity RQ, both for the SE and the ASE contributions (see Fig. 1d).

The RQ_{SE} increases from an initial value of 12% detected at low excitation density up to 25% registered at 0.75 mJ cm^{-2} and tends to saturate around 30% for higher excitation densities. This behavior is consistent with the presence of emission from trapped excitons at low excitation density, with a progressive traps saturation as the excitation density increases [50] and suggests a stronger air induced quenching of free excitons with respect to the trapped ones. The RQ_{ASE}, on the other hand, rapidly increases around the threshold from 5% to 50% and then remains constant around 52% (see Fig. 1d). The obtained results clearly testify that detecting the ASE intensity allows to increase the response up to two times, with respect to the spontaneous emission. The difference in the relative quenching between SE and ASE above threshold is due to the fact that the spontaneous emission linearly depends on the exciton density, whereas the ASE shows an exponential dependence [44,50], resulting in a stronger intensity decrease for ASE in presence of air.

The constant RQ_{ASE} above 0.75 mJ cm^{-2} suggests that the ratio between the time constant of the air-induced exciton quenching process and the ASE lifetime does not appreciably vary in the investigated excitation densities range. Differently from polymeric samples where the RQ_{ASE} was demonstrated to be strongly dependent on the excitation density [42,51], in our study the ASE quenching results independent of the excitation density, giving the possibility to exploit it for a potential device regardless the pumping conditions, thus clearing the way for possible applications of ASE gas sensing with $CsPbBr_3$ NCs.

The detection sensitivity has been determined by measuring the RQ dependence on the moisture content in the test chamber, modified by changing the test chamber pressure. The obtained results allow to observe that, both for SE and ASE, the relative quenching shows an initial linear increase, followed by a slower reduction (above 1 $\mu g/cm^3$), as reported in Figure S5. The ASE detection sensitivity, obtained from the slope of the RQ plots, is 71 $(\mu g/cm^3)^{-1}$ at low humidity concentrations. Similarly to what observed for the relative quenching, the spontaneous emission sensitivity is lower than the ASE one, with a maximum of 11 $(\mu g/cm^3)^{-1}$ at low humidity concentrations. The observed difference between the ASE and SE sensitivity confirms the stronger response of the stimulated radiation to the environment change, with S_{ASE} value

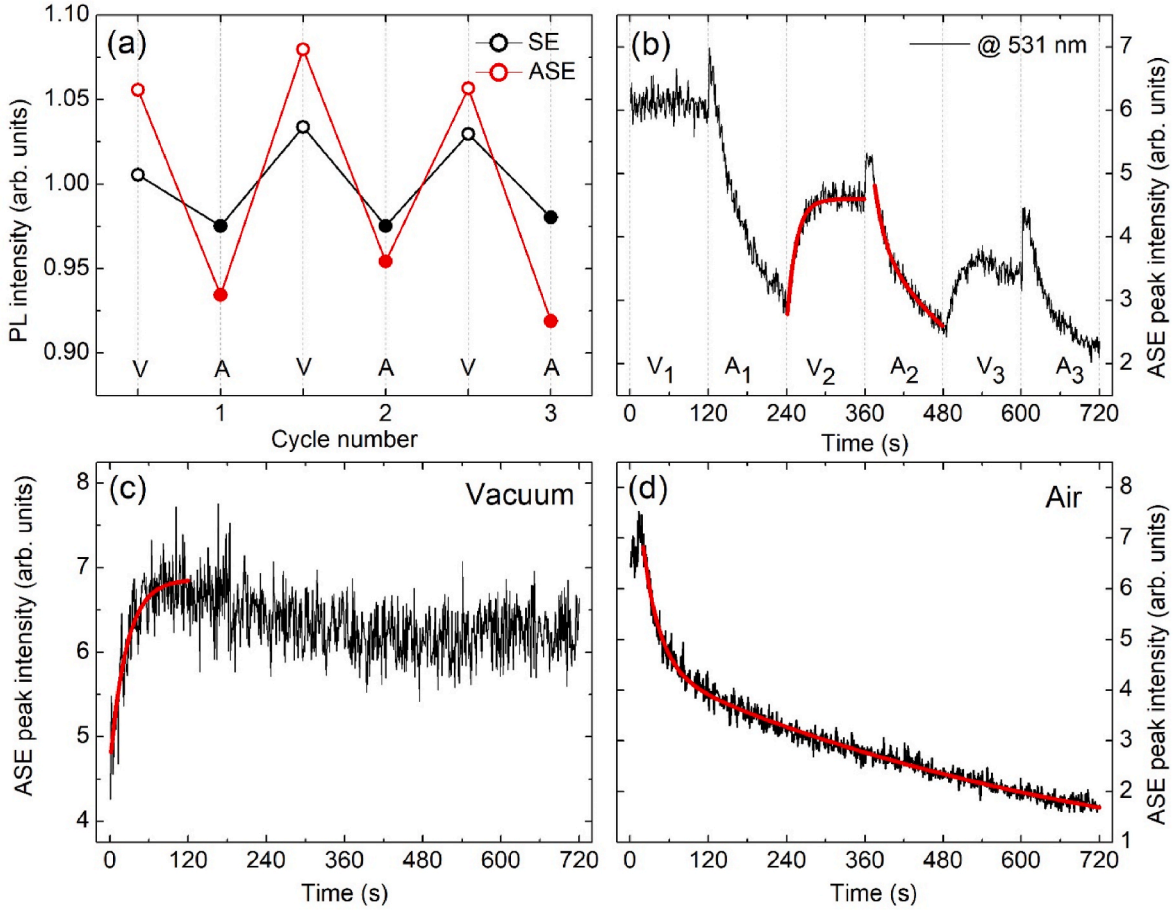

Fig. 2. (a) ASE and SE integrated intensity dependence in a static measurement from vacuum (circles) to air (dots) and vice-versa; (b) ASE peak intensity modulation in a dynamic measurement from vacuum to air; red curves are the best fit lines for vacuum recovery (V_2 time window, eq. (2)) and air decay (A_2 time window, eq. (1)) (c) ASE peak intensity recovery under continuous laser irradiation in vacuum conditions; the exponential best fit line to eq. (2) is marked in red; (d) ASE peak intensity decay under continuous laser irradiation in air; in red the bi-exponential best fit line to eq. (1). (For interpretation of the references to color in this figure legend, the reader is referred to the Web version of this article.)

up to 6.5 times higher than S_{SE} at low humidity concentrations.

We also calculated the Limit of Detection (LOD), that is the smallest humidity concentration the sample is able to distinguish from a blank reading with a stated confidence level (95%), obtaining a LOD of 46 ng/cm^3 for ASE quenching.

In order to investigate the reversibility of the emission quenching in air, we performed cyclic measurements changing the environment from vacuum to air, and then back to vacuum. For sensing tests, we chose an excitation density of about 1 mJ cm^{-2}, slightly above the ASE threshold in order to exploit ASE stronger response and simultaneously keep the sample under moderate light irradiation, avoiding sample degradation. We first performed *static* measurements, waiting 3 min between any environment change and the following acquisition of the PL spectrum. Fig. 2a shows the modulation of both the SE and the ASE integrated intensity as a function of the environment, with higher values in vacuum than in air and a stronger environmental dependence of ASE with respect to the non-stimulated radiation; the signal intensity modulation remains stable for at least 3 complete cycles. We then performed *dynamic* measurements, in which the sample was continuously pumped with laser light, and the sample environment was switched between vacuum and air every 2 min, for a total of 12 min (see Fig. 2b), identifying three vacuum time windows (V_1= (0–120) s, V_2 = (240–360) s, V_3 = (480–600) s) and three air time windows (A_1 = (120–240) s, A_2 = (360–480) s, A_3 = (600–720) s).

Starting from vacuum conditions, the ASE peak intensity remains constant for the entire time window (V_1). Then, as soon as the sample chamber is air-filled, an immediate intensity increase is detected, which is due to a mechanical artifact during the chamber filling process (about 5s), followed by a progressive intensity quenching that leads to about the halving of the initial ASE intensity in 2 min (A_1). When vacuum is restored, the ASE intensity increases in about 20 s, up to a constant value till the end of the 2 min (V_2).

$$I(t) = I_0 + I_1 \exp[-t/t_1] + I_2 \exp[-t/t_2] \quad (1)$$

well describes the intensity decrease in air observed in the air exposure time windows, resulting in a fast decay with average time of t_1 = (26.4 ±3.7) s and a slower decay of hundreds of seconds (see Fig. 2b). The PL recovery in vacuum (V_2 and V_3) has instead been fitted with the following function:

$$I(t) = I_0 + I_1\left[1 - e^{-\frac{t}{t_0}}\right] \quad (2)$$

resulting in a rise time of $t_0 = (15.8 \pm 1.1)$ s (see Fig. 2b).

Noteworthy, we observe that after each exposure to air the saturation signal shows an intensity reduction of about 25% with respect to the previous vacuum measurements value, suggesting that the ASE intensity modulation under continuous laser irradiation due to the environment change is characterized by the superposition of a fast reversible process and a slower progressive intensity decrease. The nature of the latter is studied by analyzing the temporal evolution of ASE by continuously exciting the samples for 12 min both in vacuum (Fig. 2c) and in air conditions (Fig. 2d). In particular, for the vacuum measurement we started from an air-filled chamber and switched to vacuum as soon as the measurement started; vice versa, for the air measurement the chamber was initially in vacuum and then immediately air filled at the beginning of the test. The ASE intensity dynamics in vacuum (Fig. 2c) is fully compatible with the results observed in Fig. 2b: passing from air to vacuum the ASE intensity is restored in less than a minute and remains almost constant for the entire measurement time. The first 2 min of the recovery curve have been fitted with Equation (2), obtaining t_0 = (20.0 ± 1.5) s as recovery time. On the other hand, when the sample is pumped in air, starting from vacuum (see Fig. 2d), we observe an immediate intensity increase, followed by a fast decay within the first 2 min and then by a slower one. This behavior can be reproduced by a best-fit with Equation (1), with best fit characteristic times of $t_1 = (25.3 \pm 1.1)$ s and $t_2 = (723.2 \pm 6.9)$ s (consistent with the dynamics observed on a short time scale of Fig. 2b) leading to an ASE intensity drop of about 70% after 720 s of continuous laser irradiation.

In order to study the reversibility of the slower quenching process, we recorded PL spectra every 45 min (with the sample kept in vacuum and dark, except for the excitation time of 1s for each measurement), after continuous pumping the NCs film in air for 12 min (see Fig. 3a).

Noteworthy, the obtained results show a progressive recovery of the ASE peak intensity (see Fig. 3b) well described by an exponential increase up to saturation. Fitting the experimental data to Equation (2) allowed us to extract the characteristic time t_0 of the PL recovery, obtaining as a result t_0 = (140 ±40) *min*. A full disappearance of the ASE quenching is reached after some hours, as shown in Figure S6 that compares the PL spectrum before air irradiation, the last one after 12 min of laser pumping in air and the one after about 7 h of vacuum storage. What is more, the dynamic process of the intensity recovery after long laser excitation is also present for stronger irradiation (24 min above threshold) and it is clearly visible in the PL maps of the irradiated region. After the excitation, the fluorescence map of the sample shows a clear darker trace in correspondence of the pumped stripe (see Fig. 3c) that almost completely disappears after one night of storage in dark and vacuum (see Fig. 3d). The long term self-healing character of the perovskite and the characteristic time scale of the recovery process point toward a quenching process of the PL originating from a physical (rather than chemical) mechanism such as the adsorption of water molecules under air conditions and desorption when the vacuum is restored.

The high humidity level of the air used in this experiment (60% RH) determines the solvation of the surface and the hydrophilic zwitterionic head groups, leading to the formation of non-radiative defect states, and consequently the quenching of the sample emission (both spontaneous and stimulated), with a characteristic time of the water adsorption and ligand solvation of about 20 s (short decay time after air exposure). In vacuum conditions the water molecules probably can desorb, restoring the pristine condition.

Our results evidence that this process has two characteristic times: a shorter one on the scale of few tens of seconds, that leads to the PL quenching and recovery in about 20s, and a longer one that brings to complete PL intensity recovery after a few hours.

The role of the ligand in the observed environmental dependence of the emission properties of our samples is also suggested by the differences with previous reports on $CsPbBr_3$ NCs capped with oleic acid and oleylamine [20–22]. In particular, these studies also reported an emission properties recovery after photodegradation, but our lecithin-capped nanocrystals show smaller degradation effects (limited to an intensity reduction, while oleic acid and oleylamine-capped NCs showed huge color change, from yellow to black), and much faster healing time (a few hours compared to a longer recovery from a minimum of 168 to more than 2000 h).

The evidence of lower degradation and faster recovery is consistent with the demonstrated strong adhesion of lecithin molecules to the NCs surface [32,35] that prevents NCs aggregation and ensures a better long-term stability to the NCs thin films.

In order to verify that the environmental induced intensity decrease is due to the formation of non-radiative defects in wet air conditions, we performed time resolved PL measurements, in vacuum and wet air conditions (see Fig. 4).

The obtained results allow to observe a non-exponential relaxation dynamic, well reproducible with the following tri-exponential decay [41, 52, 53]:

$$I(t) = I_0 + A_1 \exp\left[-\frac{t}{\tau_1}\right] + A_2 \exp\left[-\frac{t}{\tau_2}\right] + A_3 \exp\left[-\frac{t}{\tau_3}\right] \quad (3)$$

In particular, in vacuum conditions, the best fit decay values are: $\tau_1 = (5.51 \pm 0.24)$ ns, $\tau_2 = (12.66 \pm 0.63)$ ns and $\tau_3 = (62 \pm 10)$ ns, whereas in air: $\tau_1 = (3.51 \pm 0.17)$ ns, $\tau_2 = (8.70 \pm 0.34)$ ns and τ_3 =

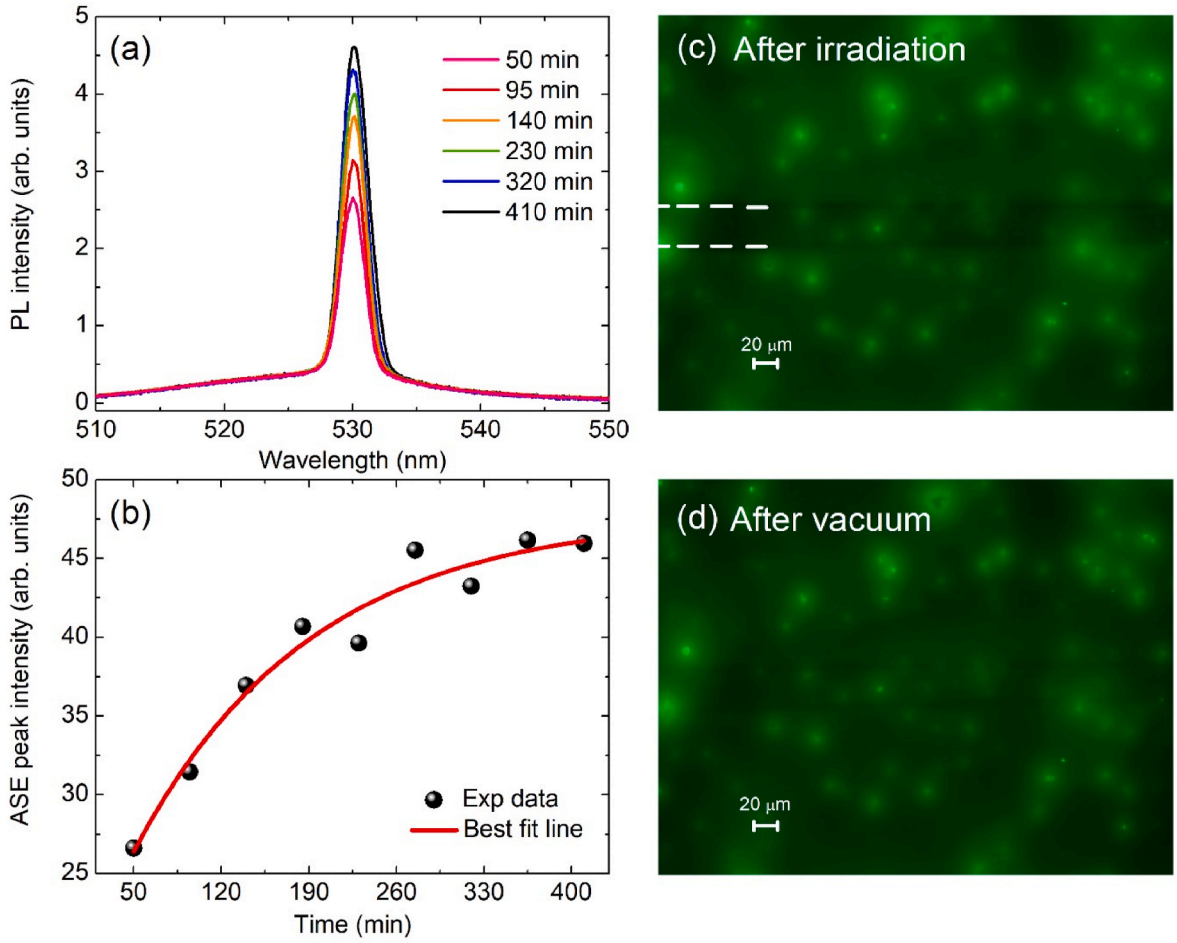

Fig. 3. (a) Temporal evolution of PL spectra and (b) ASE peak intensity recovery by storing the sample in vacuum; the red line is the best fit curve assuming an exponential recovery up to saturation value. 435 μm × 326 μm fluorescence map of the sample (c) immediately after 24 min laser excitation and (d) after one night in vacuum and dark storage; white dotted lines are guides for the eyes. (For interpretation of the references to color in this figure legend, the reader is referred to the Web version of this article.)

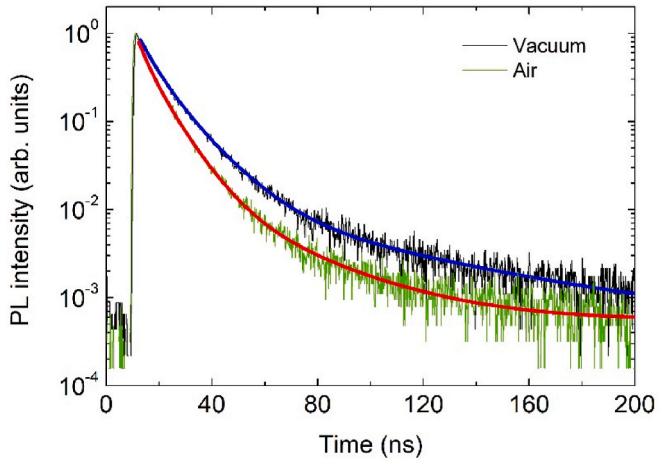

Fig. 4. TR-PL traces in vacuum (black line) and air (green line) of the NCs thin film. The blue and red lines correspond to the best fit curves with a three-exponential decay. (For interpretation of the references to color in this figure legend, the reader is referred to the Web version of this article.)

(30.6 ± 4.3) ns. The corresponding average times result: (15.8 ± 2.6) ns in vacuum and (10.2 ± 1.3) ns in air conditions, respectively. The obtained results evidence a general shortening of the decay times in air, in agreement with the introduction of a new non-radiative process when the NCs film was exposed to wet air.

4. Conclusions

In this work we investigated the environmental dependence of the ASE properties in NCs thin films of $CsPbBr_3$ perovskite. We analyzed the optical properties in vacuum and air, demonstrating optical gain with low ASE threshold in both ambient conditions. For the first time we demonstrated the higher ASE sensitivity of the perovskite NCs to the environment with respect to the non-stimulated emission up to 6.5 times, opening the way for exploiting ASE intensity modulation for optical sensing devices. Moreover, the RQ_{ASE} results independent from the excitation density, then allowing higher stability and better performances of a potential device. We also observed that the air-induced quenching of the ASE signal is fully reversible being completely restored after few hours of storage in dark and vacuum conditions, demonstrating excellent self-healing properties of the studied nanocrystal thin films. All the dynamic environmental measurements and the recovery tests suggest that the interaction between the perovskite material and the environment is of physical rather than chemical nature and rule out irreversible degradation processes. Our results thus demonstrate that $CsPbBr_3$ NCs thin films represent a particularly interesting active system for the realization of efficient ASE-based, infinitely regenerable humidity sensors.

Credit author statement

S. Milanese: Conceptualization, Methodology, Investigation, Formal Analysis, Writing – original draft, Data Curation, **G. Morello:** Conceptualization, Methodology, Investigation, Formal Analysis, Writing – original draft, Data Curation, **M. L. De Giorgi:** Conceptualization, Methodology, Investigation, Writing – Review & Editing, **A. Cretì:** Investigation, Writing – Review & Editing, **H. Andrusiv:** Resources, **M. I. Bodnarchuk:** Conceptualization, Resources, Writing – Review & Editing, **A. Qualtieri**: Investigation, Writing – Review & Editing, **M. Lomascolo:** Investigation, Writing – Review & Editing, **M. V. Kovalenko:** Conceptualization, Resources, Writing – Review & Editing, **M. Anni:** Conceptualization, Methodology, Investigation, Writing – Review & Editing, Supervision.

Declaration of competing interest

The authors declare the following financial interests/personal relationships which may be considered as potential competing interests: Maryna I. Bodnarchuk reports financial support was provided by Swiss National Science Foundation.

Data availability

Data will be made available on request.

Acknowledgments

M. I. B. acknowledge funding from the Swiss National Science Foundation (Grant No. 200021_192308, “Q-Light - Engineered Quantum Light Sources with Nanocrystal Assemblies")

Appendix A. Supplementary data

Supplementary data to this article can be found online at https://doi.org/10.1016/j.mtphys.2023.101098.

References

[1] R. Montecucco, E. Quadrivi, R. Po, G. Grancini, All-inorganic cesium-based hybrid perovskites for efficient and stable solar cells and modules, Adv. Energy Mater. 11 (23) (2021): 2100672, https://doi.org/10.1002/aenm.202100672.
[2] Q. Van Le, H.W. Jang, S.Y. Kim, Recent advances toward high-efficiency halide perovskite light-emitting diodes: review and perspective, Small Methods 2 (10) (2018): 1700419, https://doi.org/10.1002/smtd.201700419.
[3] P. Ramasamy, D.-H. Lim, B. Kim, S.-H. Lee, M.-S. Lee, J.-S. Lee, All-inorganic cesium lead halide perovskite nanocrystals for photodetector applications, Chem. Commun. 52 (2016), https://doi.org/10.1039/C5CC08643D, 2067–2070.
[4] M.L. De Giorgi, M. Anni, Amplified spontaneous emission and lasing in lead halide perovskites: state of the art and perspectives, Appl. Sci. 9 (2019) 21, https://doi.org/10.3390/app9214591.
[5] M.L. De Giorgi, M. Anni, Amplified spontaneous emission in low dimensional lead halide perovskites: an overview, Opt. Mater. X 12 (2021), https://doi.org/10.1016/j.omx.2021.100115.
[6] M.L. De Giorgi, S. Milanese, A. Klini, M. Anni, Environment-induced reversible modulation of optical and electronic properties of lead halide perovskites and possible applications to sensor development: a review, Molecules 26 (3) (2021), https://doi.org/10.3390/molecules26030705.
[7] B.W. Park, S.I. Seok, Intrinsic instability of inorganic–organic hybrid halide perovskite materials, Adv. Mater. 31 (20) (2019): 1805337, https://doi.org/10.1002/adma.201805337.
[8] J. Deng, J. Li, Z. Yang, M. Wang, All-inorganic lead halide perovskites: a promising choice for photovoltaics and detectors, J. Mater. Chem. C 7 (2019) 12415–12440, https://doi.org/10.1039/C9TC04164H.
[9] L. Protesescu, S. Yakunin, M.I. Bodnarchuk, F. Krieg, R. Caputo, C.H. Hendon, R. X. Yang, A. Walsh, M.V. Kovalenko, Nanocrystals of cesium lead halide perovskites ($CsPbX_3$, X = Cl, Br, and I): novel optoelectronic materials showing bright emission with wide color gamut, Nano Lett. 15 (6) (2015) 3692–3696, https://doi.org/10.1021/nl5048779.
[10] N. Falsini, A. Ristori, F. Biccari, N. Calisi, G. Roini, P. Scardi, S. Caporali, A. Vinattieri, A new route for caesium lead halide perovskite deposition, J. Eur. Opt. Soc.-Rapid Publ. 17 (8) (2021), https://doi.org/10.1186/s41476-021-00153-y, 1.
[11] N.E. Wright, X. Qin, J. Xu, L.L. Kelly, S.P. Harvey, M.F. Toney, V. Blum, A.D. Stiff Roberts, Influence of annealing and composition on the crystal structure of mixed-halide, Ruddlesden-Popper perovskites, Chem. Mater. 34 (7) (2022) 3109–3122, https://doi.org/10.1021/acs.chemmater.1c04213.
[12] R.L.Z. Hoye, J. Hidalgo, R.A. Jagt, J.-P. Correa-Baena, T. Fix, J.L. MacManus-Driscoll, The role of dimensionality on the optoelectronic properties of oxide and halide perovskites, and their halide derivatives, Adv. Energy Mater. 12 (4) (2022): 2100499, https://doi.org/10.1002/aenm.202100499.
[13] M.M. Elsenety, M. Antoniadou, N. Balis, A. Kaltzoglou, L. Sygellou, A. Stergiou, N. Tagmatarchis, P. Falaras, Stability improvement and performance reproducibility enhancement of perovskite solar cells following (FA/MA/Cs) $PbI_{3-x}Br_x/(CH_3)_3SPbI_3$ dimensionality engineering, ACS Appl. Energy Mater. 3 (3) (2020) 2465–2477, https://doi.org/10.1021/acsaem.9b02117.
[14] T. Seewald, E.R. Schütz, C. Ebenhoch, L. Schmidt-Mende, Curing perovskites—a way towards control of crystallinity and improved stability, JPhys Energy 2 (2) (2020): 021001, https://doi.org/10.1088/2515-7655/ab604b.
[15] T. Du, S.R. Ratnasingham, F.U. Kosasih, T.J. Macdonald, L. Mohan, A. Augurio, H. Ahli, C.-T. Lin, S. Xu, W. Xu, R. Binions, C. Ducati, J.R. Durrant, J. Briscoe, M. A. McLachlan, Aerosol assisted solvent treatment: a universal method for performance and stability enhancements in perovskite solar cells, Adv. Energy Mater. 11 (33) (2021): 2101420, https://doi.org/10.1002/aenm.202101420.
[16] S. Mariotti, O.S. Hutter, L.J. Phillips, P.J. Yates, B. Kundu, K. Durose, Stability and performance of $CsPbI_2Br$ thin films and solar cell devices, ACS Appl. Mater. Interfaces 10 (4) (2018) 3750–3760, https://doi.org/10.1021/acsami.7b14039.
[17] B.T. Diroll, G. Nedelcu, M.V. Kovalenko, R.D. Schaller, High-temperature photoluminescence of $CsPbX_3$ (X = Cl, Br, I) nanocrystals, Adv. Funct. Mater. 27 (21) (2017): 1606750, https://doi.org/10.1002/adfm.201606750.
[18] Z. Wang, Y. Zhang, X. Liu, Y. Yu, F. Xu, J. Ding, X. Liang, K. Yang, W. Xiang, High stability and strong luminescence $CsPbBr_3/Cs_4PbBr_6$ perovskite nanocomposite: large-scale synthesis, reversible luminescence, and anti-counterfeiting application, Adv. Mater. Technol. 6 (12) (2021): 2100654, https://doi.org/10.1002/admt.202100654.
[19] D.R. Ceratti, Y. Rakita, L. Cremonesi, R. Tenne, V. Kalchenko, M. Elbaum, D. Oron, M.A.C. Potenza, G. Hodes, D. Cahen, Self-healing inside $APbBr_3$ halide perovskite crystals, Adv. Mater. 30 (10) (2018): 1706273, https://doi.org/10.1002/adma.201706273.
[20] K. Kidokoro, Y. Iso, T. Isobe, Complete self-recovery of photoluminescence of photodegraded cesium lead bromide quantum dots, J. Mater. Chem. C 7 (2019) 8546–8550, https://doi.org/10.1039/C9TC02365H.
[21] K. Miyashita, K. Kidokoro, Y. Iso, T. Isobe, Effects of halide composition on the self-recovery of photodegraded cesium lead halide perovskite nanocrystals: implications for photoluminescence applications, ACS Appl. Nano Mater. 4 (11) (2021) 12600–12608, https://doi.org/10.1021/acsanm.1c03119.
[22] I. Enomoto, Y. Iso, T. Isobe, Implications of gas-barrier properties in realizing the self-recovery of photodegraded $CsPbBr_3$ perovskite nanocrystals, J. Mater. Chem. C 10 (2022) 102–107, https://doi.org/10.1039/D1TC05077J.
[23] A. Argyrou, K. Brintakis, A. Kostopoulou, E. Gagaoudakis, I. Demeridou, V. Binas, G. Kiriakidis, E. Stratakis, Highly sensitive ozone and hydrogen sensors based on perovskite microcrystals directly grown on electrodes, Journal of Materiomics 8 (2) (2022) 446–453, https://doi.org/10.1016/j.jmat.2021.07.002.
[24] H. Chen, M. Zhang, R. Bo, C. Barugkin, J. Zheng, Q. Ma, S. Huang, A.W.Y. Ho-Baillie, K.R. Catchpole, A. Tricoli, Superior self-powered room-temperature chemical sensing with light-activated inorganic halides perovskites, Small 14 (7) (2018): 1702571, https://doi.org/10.1002/smll.201702571.
[25] K.K. Chan, S.H.K. Yap, D. Giovanni, T.C. Sum, K.-T. Yong, Water-stable perovskite quantum dots-based fret nanosensor for the detection of rhodamine 6G in water, food, and biological samples, Microchem. J. 180 (2022): 107624, https://doi.org/10.1016/j.microc.2022.107624.
[26] E. Aznar-Gadea, I. Sanchez-Alarcon, A. Soosaimanickam, P.J. Rodriguez-Canto, F. Perez-Pla, J.P. Martínez-Pastor, R. Abargues, Molecularly imprinted nanocomposites of $CsPbBr_3$ nanocrystals: an approach towards fast and selective gas sensing of explosive taggants, J. Mater. Chem. C 10 (2022) 1754–1766, https://doi.org/10.1039/D1TC05169E.
[27] J. Guan, Y.-z. Shen, Y. Shu, D. Jin, Q. Xu, X.-Y. Hu, Internal–external stabilization strategies enable ultrastable and highly luminescent $CsPbBr_3$ perovskite nanocrystals for aqueous Fe^{3+} detection and information encryption, Adv. Mater. Interfac. 8 (19) (2021): 2100588, https://doi.org/10.1002/admi.202100588.
[28] D. Di Girolamo, M.I. Dar, D. Dini, L. Gontrani, R. Caminiti, A. Mattoni, M. Graetzel, S. Meloni, Dual effect of humidity on cesium lead bromide: enhancement and degradation of perovskite films, J. Mater. Chem. 7 (2019) 12292–12302, https://doi.org/10.1039/C9TA00715F.
[29] G. Niu, X. Guo, L. Wang, Review of recent progress in chemical stability of perovskite solar cells, J. Mater. Chem. 3 (2015) 8970–8980, https://doi.org/10.1039/C4TA04994B.
[30] M. Kulbak, S. Gupta, N. Kedem, I. Levine, T. Bendikov, G. Hodes, D. Cahen, Cesium enhances long-term stability of lead bromide perovskite-based solar cells, J. Phys. Chem. Lett. 7 (1 167–172) (2016), https://doi.org/10.1021/acs.jpclett.5b02597.
[31] R.E. Beal, D.J. Slotcavage, T. Leijtens, A.R. Bowring, R.A. Belisle, W.H. Nguyen, G. F. Burkhard, E.T. Hoke, M.D. McGehee, Cesium lead halide perovskites with improved stability for tandem solar cells, J. Phys. Chem. Lett. 7 (5) (2016) 746–751, https://doi.org/10.1021/acs.jpclett.6b00002.
[32] F. Krieg, S.T. Ochsenbein, S. Yakunin, S. ten Brinck, P. Aellen, A. Süess, B. Clerc, D. Guggisberg, O. Nazarenko, Y. Shynkarenko, S. Kumar, C.-J. Shih, I. Infante, M. V. Kovalenko, Colloidal $CsPbX_3$ (X = Cl, Br, I) nanocrystals 2.0: zwitterionic capping ligands for improved durability and stability, ACS Energy Lett. 3 (3) (2018) 641–646, https://doi.org/10.1021/acsenergylett.8b00035.

[33] Q.A. Akkerman, G. Rainò, M.V. Kovalenko, L. Manna, Genesis, challenges and opportunities for colloidal lead halide perovskite nanocrystals, Nat. Mater. 17 (2018) 394–405, https://doi.org/10.1038/s41563-018-0018-4.
[34] S.-Q. Sun, X.-C. Hua, Q.-W. Liu, T.-T. Wang, W. Luo, Y.-J. Zhang, L.-S. Liao, M.-K. Fung, Influence of a lecithin additive on performance of all-inorganic perovskite light-emitting diodes, J. Mater. Chem. C 7 (2019) 2905, https://doi.org/10.1039/c8tc06365f.
[35] F. Krieg, Q.K. Ong, M. Burian, G. Rainò, D. Naumenko, H. Amenitsch, A. Süess, M. J. Grotevent, F. Krumeich, M.I. Bodnarchuk, I. Shorubalko, F. Stellacci, M. V. Kovalenko, Stable ultraconcentrated and ultradilute colloids of CsPbX3 (X = Cl, Br) nanocrystals using natural lecithin as a capping ligand, J. Am. Chem. Soc. 141 (50) (2019), https://doi.org/10.1021/jacs.9b09969, 19839–19849.
[36] W.J. Mir, A. Alamoudi, J. Yin, K.E. Yorov, P. Maity, R. Naphade, B. Shao, J. Wang, M.N. Lintangpradipto, S. Nematulloev, A.-H. Emwas, A. Genovese, O. F. Mohammed, O.M. Bark, Lecithin capping ligands enable ultrastable perovskite-phase $CsPbI_3$ quantum dots for Rec. 2020 bright-red light-emitting diodes, J. Am. Chem. Soc. 144 (2022) 13302–13310, https://doi.org/10.1021/jacs.2c04637.
[37] J.R. Harwell, J.M.E. Glackin, N.J.L.K. Davis, R.N. Gillanders, D. Credgington, G. A. Turnbull, I.D.W. Samuel, Sensing of explosive vapor by hybrid perovskites: effect of dimensionality, Apl. Mater. 8 (7) (2020): 071106, https://doi.org/10.1063/5.0011229.
[38] S. Yakunin, L. Protesescu, F. Krieg, M.I. Bodnarchuk, G. Nedelcu, M. Humer, G. De Luca, M. Fiebig, W. Heiss, M.V. Kovalenko, Low-threshold amplified spontaneous emission and lasing from colloidal nanocrystals of cesium lead halide perovskites, Nat. Commun. 6 (2015) 8056, https://doi.org/10.1038/ncomms9056.
[39] M. Lorenzon, L. Sortino, Q. Akkerman, S. Accornero, J. Pedrini, M. Prato, V. Pinchetti, F. Meinardi, L. Manna, S. Brovelli, Role of nonradiative defects and environmental oxygen on exciton recombination processes in $CsPbBr_3$ perovskite nanocrystals, Nano Lett. 17 (6) (2017) 3844–3853, https://doi.org/10.1021/acs.nanolett.7b01253.
[40] H. Huang, M. Hao, Y. Song, S. Dang, X. Liu, Q. Dong, Dynamic passivation in perovskite quantum dots for specific ammonia detection at room temperature, Small 16 (6) (2020): 1904462, https://doi.org/10.1002/smll.201904462.
[41] M. Anni, A. Cretì, Y. Zhang, M.L. De Giorgi, M. Lomascolo, Investigation of the role of the environment on the photoluminescence and the exciton relaxation of $CsPbBr_3$ nanocrystals thin films, Appl. Sci. 10 (6) (2020), https://doi.org/10.3390/app10062148.
[42] A. Rose, Z. Zhu, C.F. Madigan, T.M. Swager, V. Bulović, Sensitivity gains in chemosensing by lasing action in organic polymers, Nature 434 (2005) 876–879, https://doi.org/10.1038/nature03438.
[43] M. Guillén, F. Gámez, T. Lopes-Costa, J. Castro-Smirnov, R. Wannemacher, J. Cabanillas-González, J. Pedrosa, Amplified spontaneous emission in action: sub-ppm optical detection of acid vapors in poly[2-methoxy-5-(2-ethylhexyloxy)-1,4-phenylenevinylene] thin films, Sens. Actuators, B 255 (2018) 1354–1361, https://doi.org/10.1016/j.snb.2017.08.136.
[44] W. Chen, X. Lu, F. Fan, J. Du, Optical-gain-based sensing using inorganic-ligand-passivated colloidal quantum dots, Nano Lett. 21 (18) (2021) 7732–7739, https://doi.org/10.1021/acs.nanolett.1c02547.
[45] S. Milanese, M.L. De Giorgi, L. Cerdán, M.-G. La-Placa, N.F. Jamaludin, A. Bruno, H.J. Bolink, M.V. Kovalenko, M. Anni, Amplified spontaneous emission threshold dependence on determination method in dye-doped polymer and lead halide perovskite waveguides, Molecules 27 (13) (2022), https://doi.org/10.3390/molecules25132992.
[46] A. Balena, A. Perulli, M. Fernandez, M.L. De Giorgi, G. Nedelcu, M.V. Kovalenko, M. Anni, Temperature dependence of the Amplified Spontanous Emission from $CsPbBr_3$ nanocrystal thin films, J. Phys. Chem. C 122 (10) (2018) 5813–5819, https://doi.org/10.1021/acs.jpcc.8b01419.
[47] M.L. De Giorgi, F. Krieg, M.V. Kovalenko, M. Anni, Amplified Spontaneous Emission threshold reduction and operational stability improvement in $CsPbBr_3$ nanocrystals films by hydrophobic functionalization of the substrate, Sci. Rep. 9 (2019): 17964, https://doi.org/10.1038/s41598-019-54412-7.
[48] S. Huang, L. Wang, M. Lyu, J. Zhang, J. Zhu, Effect of surface ligand density on the amplified spontaneous emission properties of $CsPbI_2Br$ quantum dots, Opt. Mater. 137 (2023): 113515, https://doi.org/10.1016/j.optmat.2023.113515.
[49] Z. Zhao, O. Mhibik, M. Nafa, S. Chénais, S. Forget, High brightness diode-pumped organic solid-state laser, Appl. Phys. Lett. 106 (2015): 051112, https://doi.org/10.1063/1.4907318.
[50] G. Xing, N. Mathews, S.S. Lim, N. Yantara, X. Liu, D. Sabba, M. Grätzel, S. Mhaisalkar, T.C. Sum, Low-temperature solution-processed wavelength-tunable perovskites for lasing, Nat. Mater. 13 (2014) 476–480, https://doi.org/10.1038/nmat3911.
[51] M. Anni, S. Lattante, Excitation density dependence of optical oxygen sensing in poly(9,9-dioctylfluorene) waveguides showing amplified spontaneous emission, ISRN Mater. Sci. 856716 (2014) 2014, https://doi.org/10.1155/2014/856716.
[52] J. Li, X. Yuan, P. Jing, J. Li, M. Wei, J. Hua, J. Zhao, L. Tian, Temperature-dependent photoluminescence of inorganic perovskite nanocrystal films, RSC Adv. 6 (2016): 78311, https://doi.org/10.1039/c6ra17008k.
[53] S. Sun, D. yuan, Y. Xu, A. Wang, Z. Deng, Ligand-mediated synthesis of shape-controlled cesium lead halide perovskite nanocrystals via reprecipitation process at room temperature, ACS Nano 10 (2016) 3648–3657, https://doi.org/10.1021/acsnano.5b08193.